Investigation of structure in ^{23}Al via resonant proton scattering of ^{22}Mg+p and the ^{22}Mg(p, γ) ^{23}Al astrophysical reaction rate

J. J. He,[1,*] S. Kubono,[1] T. Teranishi,[1,†] M. Notani,[1,‡] H. Baba,[1,2] S. Nishimura,[2] J. Y. Moon,[3] M. Nishimura,[2] H. Iwasaki,[1,4] Y. Yanagisawa,[2] N. Hokoiwa,[5] M. Kibe,[5] J. H. Lee,[3] S. Kato,[6] Y. Gono,[5] and C. S. Lee[3]

[1]*Center for Nuclear Study (CNS), University of Tokyo, Wako Branch at RIKEN, 2-1 Hirosawa, Wako, Saitama 351-0198, Japan*

[2]*RIKEN (The Institute of Physical and Chemical Research), 2-1 Hirosawa, Wako, Saitama 351-0198, Japan*

[3]*Department of Physics, Chung-Ang University, Seoul 156-756, Republic of Korea*

[4]*Department of Physics, University of Tokyo, 7-3-1 Hongo, Bunkyo, Tokyo 113-0033, Japan*

[5]*Department of Physics, Kyushu University, 6-10-1 Hakozaki, Fukuoka 812-8581, Japan*

[6]*Department of Physics, Yamagata University, Yamagata 990-8560, Japan*

(Received 15 May 2007; revised manuscript received 18 September 2007; published 5 November 2007)

Proton resonant states in ^{23}Al have been investigated for the first time by the resonant elastic and inelastic scattering of ^{22}Mg+p with a ^{22}Mg beam at 4.38 MeV/nucleon bombarding a thick $(CH_2)_n$ target. The low-energy ^{22}Mg beam was separated by the CNS radioactive ion beam separator (CRIB). The energy spectra of recoiled protons were measured at average scattering angles of $\theta_{lab} \approx 4^\circ$, 17° and 23°. A new state has been observed at $E_x = 3.00$ MeV with a spin-parity assignment of $(3/2^+)$. In addition, resonant inelastic scattering has populated three more states at excitation energies of 3.14, 3.26, and 3.95 MeV, with proton decay to the first excited state in ^{22}Mg being observed. The new state at 3.95 MeV has been assigned a spin-parity of $J^\pi = (7/2^+)$. The resonant parameters were determined by an R-matrix analysis of the excitation functions with a SAMMY-M6-BETA code. The core-excited structure of ^{23}Al is discussed within a shell-model picture. The stellar reaction rate of the ^{22}Mg(p, γ)^{23}Al reaction has been reevaluated, and the revised total reaction rate is about 40% greater than the previous result for temperatures beyond $T_9 = 0.3$.

DOI: 10.1103/PhysRevC.76.055802 PACS number(s): 25.60.−t, 23.50.+z, 26.50.+x, 27.30.+t

I. INTRODUCTION

In the field of nuclear physics, the structure of ^{23}Al is still largely unknown despite its importance to the physics of exotic nuclei—it lies four neutrons away from the line of stability. The excited states in ^{23}Al have been studied by the ^{24}Mg(^{7}Li, ^{8}He)^{23}Al reaction [1,2], the β-delayed proton decay of ^{23}Si [3,4], and the Coulomb dissociation of ^{23}Al [5,6]. However, proton resonant states in ^{23}Al cannot necessarily be excited by the (^{7}Li, ^{8}He) reaction because of the different reaction mechanism, the β-delayed proton-decay study of ^{23}Si is restricted by the selection rules, and the reported level scheme and spin-parity assignments in ^{23}Al are possibly not very reliable because the final state in ^{22}Mg was not identified. The Coulomb-dissociation experiment only studied the first and the second excited states in ^{23}Al. Interestingly, a proton halo structure with a $J^\pi = 1/2^+$ assignment has been suggested for the ground state in ^{23}Al [7,8], while recent studies have claimed the ground state to have a (normal) spin-parity of $5/2^+$ [9,10]. The recent compilations for $A = 23$ nuclei can be found in Refs. [11,12], and it can be seen that several states have been reported in ^{23}Al, although most of them have no firm spin-parity assignment. In addition, the proton separation energy of ^{23}Al is very small, $S_p = 0.123$ MeV [1]; whereas that of ^{22}Mg is 5.502 MeV [13]. Consequently, ^{22}Mg can be considered as a core in ^{23}Al, and thereby the low-lying nuclear structure in ^{23}Al can be interpreted as a simple core plus single-particle coupling picture.

In the field of nuclear astrophysics, the determination of the ^{22}Mg(p, γ)^{23}Al reaction rate is very useful for reliably predicting ^{22}Na synthesis in novae. The Ne-Na cycle, one of the noticeable reaction sequences in Ne novae [14], contains a reaction sequence of ^{20}Ne(p, γ)^{21}Na(p, γ)^{22}Mg($\beta^+\upsilon$)^{22}Na, and the ^{22}Mg(p, γ)^{23}Al reaction is one of the escape reactions from this chain. Great effort has been made to observe the characteristic ^{22}Na ($E_\gamma = 1.275$ MeV) activities with satellite-based γ-ray telescopes such as COMPTEL and has yielded an upper limit [15]. Therefore, improvements both from theory and experiment aspects are required to address the observation results. Gomi *et al*. [6] have concluded that the main reaction flow favors β decay rather than proton capture on ^{22}Mg assuming the temperature and density conditions given by the nova models [16]. In this work, the rate of the ^{22}Mg(p, γ)^{23}Al reaction has been reevaluated by using the available experimental data.

We explain the experimental setups in Sec. II and the experimental results and R-matrix analysis in Sec. III. The model calculations are presented in Sec. IV, and the level properties are discussed in Sec. V. The astrophysical reaction rate in the ^{22}Mg(p, γ)^{23}Al reaction is presented in Sec. VI.

II. EXPERIMENT

The experiment was performed using the CNS radioactive ion beam separator (CRIB) [17,18], installed by the Center

*Present address: School of Physics, University of Edinburgh, Mayfield Road, Edinburgh, EH9 3JZ, UK.

†Present address: Department of Physics, Kyushu University, 6-10-1 Hakozaki, Fukuoka 812-8581, Japan.

‡Present address: Argonne National Laboratory, 9700 S. Cass Ave., Argonne, Illinois 60439, USA.

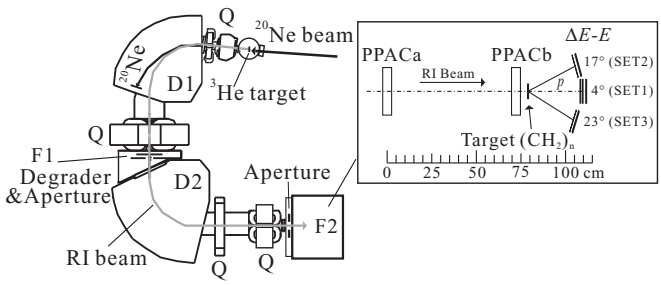

FIG. 1. Experimental setup for the scattering measurement.

for Nuclear Study (CNS), University of Tokyo, in the RIKEN Accelerator Research Facility. A primary beam of $^{20}Ne^{8+}$ was accelerated up to 8.11 MeV/nucleon by the cyclotron ($K = 70$) [19] with an average intensity of 200 pnA. The primary beam bombarded a water-cooled ^{3}He gas target confined in a small cylindrical chamber whose entrance and exit windows were made of two 2.2-μm thick Havar foils. The thickness of ^{3}He gas was 0.36 mg/cm^2 at 1-atm pressure. A secondary beam of ^{22}Mg was produced via the ^{3}He(^{20}Ne, ^{22}Mg)n reaction in inverse kinematics. In addition, a ^{21}Na radioactive beam was produced simultaneously. Both of them were separated and used in the experiment. The experimental results with the ^{21}Na beam will be discussed elsewhere [20].

The experimental setup is shown in Fig. 1. The secondary $^{22}Mg^{12+}$ particles were separated by the CRIB. At the momentum dispersive focal plane (F1), an energy degrader of 6-μm thick Mylar foil was installed to remove the background light ions from the secondary beam. After energy degradation, a horizontal aperture selected the $^{22}Mg^{12+}$ particles at a mean energy of 5.93 MeV/nucleon with a momentum spread of $\pm 0.5\%$.

At the achromatic focal plane (F2), a scattering setup was installed inside a vacuum chamber (inset of Fig. 1). The setup consisted of two parallel-plate avalanche counters (PPACs) [21], a polyethylene $(CH_2)_n$ target of 7.9 mg/cm^2, and three sets of ΔE-E silicon telescopes. The PPAC was used for measuring time and two-dimensional position information of the particles. The beam profile on the secondary target was also monitored by the PPACs during the data acquisition. The beam particles were identified in an event-by-event mode by using the time of flight (TOF) between two PPACs, and the TOF between PPACb and the rf signal provided by the cyclotron. At target position, the average intensity of the ^{22}Mg beam was 4.4×10^3 particles/s with a purity of about 3%. The major contaminant in the radioactive ion (RI) beam was ^{20}Ne caused by scattering of the primary beam at the inner walls of the magnets. The ^{22}Mg beam-spot widths (full width at half maximum, FWHM) were 15 mm horizontally and 11 mm vertically. The horizontal and vertical angular widths (FWHM) of the beam were 28 and 33 mrad, respectively. The mean energy of ^{22}Mg was 4.38 MeV/nucleon with a width (FWHM) of 0.18 MeV/nucleon on the target.

The ^{22}Mg particles were fully stopped in the $(CH_2)_n$ target, thus Si detectors did not face the beam directly. The ΔE-E telescopes were placed at three scattering angles for measuring the recoil products, e.g., p, d, α, and other light particles. To facilitate the following description, the ΔE-E telescopes at averaged angles of $\theta_{\rm lab} \approx 4^\circ, 17^\circ$, and 23° are referred to as SET1, SET2, and SET3, respectively (see Fig. 1). The scattering angle in the center-of-mass system can be deduced by $\theta_{\rm c.m.} = 180^\circ - 2\theta_{\rm lab}$ in the elastic scattering case. As for SET1, a double-sided-strip (16×16 strips) ΔE was used for measuring the two-dimensional position information; while for ΔE in SET2 and SET3, only horizontal strips were used. By using the proton-hit position on the ΔE detector and the PPAC position information, the resolution of the scattering angle was determined to be 1.0°, 1.4°, and 1.3° (FWHM) for SET1, SET2, and SET3, respectively. The recoiled protons were clearly identified by ΔE-E and E_p-TOF information. Here, TOF is the time of flight between PPACb and the corresponding ΔE detector. The total proton energy (E_p) was deduced from the energies measured by ΔE-E telescopes. The energy calibration for the detector system was performed using the secondary proton beams separated by CRIB at several energy points.

Experimental data with a C target (9.3 mg/cm^2) was also acquired in a separate run to evaluate the contributions from the reactions of ^{22}Mg with C nuclei. The yield ratio of these two proton spectra [with $(CH_2)_n$ and C targets] was normalized by the number of beam particles and by the target thickness per unit beam energy loss in the corresponding targets.

III. RESULTS

A. Experimental results

For reverse kinematics, the center-of-mass energy $E_{\rm c.m.}$ of the ^{22}Mg+p system is related to the energy E_p of the recoil protons detected at a laboratory angle $\theta_{\rm lab}$ by

$$E_{\rm c.m.} = \frac{A_b + A_t}{4A_b \cos^2\theta_{\rm lab}} E_p, \qquad (1)$$

where A_b and A_t are the mass numbers of the beam and target nuclei. This equation is valid only for an elastic scattering case. Practically, E_p was converted to $E_{\rm c.m.}$ by assuming the elastic scattering kinetics and considering the energy loss of particles in the target. The energy resolution of $E_{\rm c.m.}$ was determined by the resolution of the Si telescope system, the angular resolution of the scattering angle, the energy width of the secondary beam, and the particle straggling in the target material. The energy resolution of the detection system was the main source in all three SETs. The overall energy resolution (FWHM) of $E_{\rm c.m.}$ in SET1 was about 20 keV (at 0.5 MeV) to 45 keV (at 3.5 MeV). While those in SET2 and SET3 were about 20–70 keV, because the larger scattering angle resulted in larger kinetic shifts. The systematic errors of $E_{\rm c.m.}$ were caused mainly by the uncertainties of proton energy calibration. In SET1, it was about $\pm$12 keV (at 1.0 MeV) to $\pm$20 keV (at 3.5 MeV), and about $\pm$13 to $\pm$30 keV in SET2 and $\pm$15 to $\pm$40 keV in SET3.

Figure 2 shows experimental proton spectra for ^{22}Mg+p scattering at $\theta_{\rm c.m.} = 172^\circ$ (i.e., $\theta_{\rm lab} = 4^\circ$ with SET1). All the spectra were corrected for proton energy loss in exiting the target. To deduce the energy scale, the kinematics of elastic scattering of ^{22}Mg+p was assumed. The upper histogram was obtained with the $(CH_2)_n$ target exposed to the beam, while for the lower one a pure C target was used. Data in the dead layer region (between ΔE and E detectors)

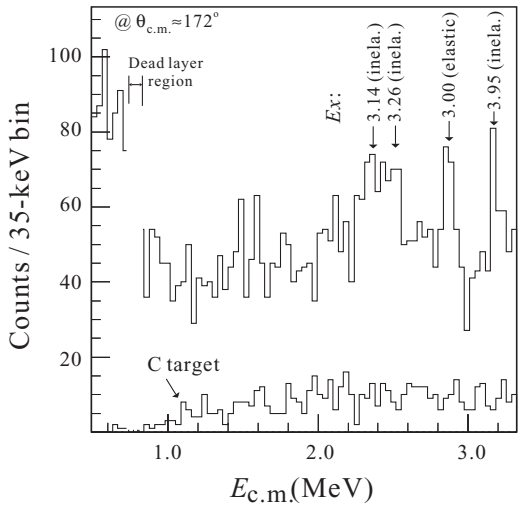

FIG. 2. Experimental proton spectrum for ^{22}Mg+p elastic scattering at $\theta_{\text{c.m.}} = 172^{\circ}$.

were removed as indicated in the figure. The resonances seen in Fig. 2 have been fitted using a Lorentzian function, resulting in the resonance energy determinations shown. Corresponding excitation energies in ^{23}Al can be calculated by $E_x = E_{\text{c.m.}} + 0.123$ (in MeV). Blank *et al.* [3] have reported that certain excited states in ^{23}Al decay to the first excited state in ^{22}Mg by proton emission. Consequently, the resonant inelastic scattering contribution also has to be considered. In the present experiment, both resonant elastic and inelastic scattering events have been clearly identified. The kinematics analysis approach used to do this is explained below.

Since the aforementioned spectra were obtained under the assumption of kinematics describing elastic scattering of ^{22}Mg+p, one expects that the c.m. energies at which true elastic scattering peaks occur will be constant regardless of the scattering angle. Conversely, peaks that are in fact due to inelastic scattering will appear at an energy that depends on scattering angle. Figure 3 illustrates the power of this technique and clearly identifies those resonances at 3.14, 3.26, and 3.95 MeV as being due to inelastic scattering, while the elastic resonance at 3.00 MeV stays within the error bar. The thick

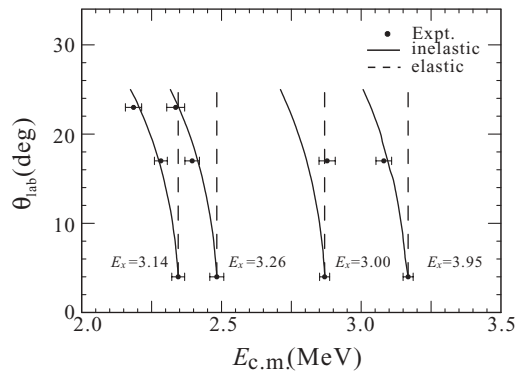

FIG. 3. Scattering center-of-mass energies $E_{\text{c.m.}}$ vs scattering angle. $E_{\text{c.m.}}$ is derived under the assumption of elastic scattering kinematics of ^{22}Mg+p. See text for details.

solid lines indicate the calculated kinematics for the inelastic case, i.e., decaying into the first excited state ($J^{\pi} = 2^{+}$, 1.25 MeV) in ^{22}Mg by the emission of a proton, while the dashed lines indicate the angle independent elastic case. Furthermore, the magnitude of the kinematic energy shift from the elastic scattering (the dashed line in Fig. 3) depends on the excitation energy in the ^{22}Mg nucleus; that is, the higher the excitation energy, the larger the energy shift. If one measures precisely the energy shift, the excitation energy of the core can be determined. As a conclusion, the 3.00 MeV state decays to the ground state, while the states at 3.14, 3.26, and 3.95 MeV decay predominantly to the 1.25 MeV first excited state in ^{22}Mg.

A new level scheme of ^{23}Al is proposed in Fig. 4. The uncertainty in the energies is indicated by the number in parentheses; it includes both systematic and fitting uncertainties and is given in keV. The previously observed states are also shown for comparison. It can be concluded that the 3.00 and 3.95 MeV states are newly observed, and the states at 3.14 and 3.26 MeV could correspond to the broad peak at $E_x = 3.204$ MeV reported before [1].

B. *R*-matrix analysis

The laboratory differential cross sections ($d\sigma/d\Omega$) for ^{22}Mg+p scattering at energy E_p and angle θ_{lab} are deduced [22] from the proton spectrum by

$$\frac{d\sigma}{d\Omega_{\text{lab}}}(E_p, \theta_{\text{lab}}) = \frac{N}{I_0 N_s \Delta\Omega_{\text{lab}}}, \tag{2}$$

where N is the number of detected protons, i.e., at energy interval of $E_p \rightarrow E_p + \Delta E$ and scattering angle of θ_{lab}, which are measured by a Si telescope covering a solid angle $\Delta\Omega_{\text{lab}}$. I_0 is the total number of ^{22}Mg beam particles bombarding the $(CH_2)_n$ target and is considered to be constant in the whole energy region. The correction of dead time has been made properly here. N_s is the number of H atoms per unit area per energy bin in the target (dx/dE) [23]. The transformation of the laboratory differential cross sections to the c.m. frame is given by

$$\frac{d\sigma}{d\Omega_{\text{c.m.}}}(E_{\text{c.m.}}, \theta_{\text{c.m.}}) = \frac{1}{4\cos\theta_{\text{lab}}} \frac{d\sigma}{d\Omega_{\text{lab}}}(E_p, \theta_{\text{lab}}). \tag{3}$$

Because the main error in cross-section data is statistical, about 15%, and systematic error is estimated to be less than 6%, only statistical error is taken into account in the present work.

The c.m. differential cross sections have been analyzed by an R-matrix [24] code SAMMY-M6-BETA [25], which enables multilevel R-matrix fits to the cross-section data using Bayes's equations. The Reich-Moore approximation [26] is used in the code, i.e., neglecting the level-level interference for the capture channels and neglecting interference between the aggregate capture channel and other channels. The R matrix takes the form of

$$R_{cc'} = \sum_{\lambda} \frac{\gamma_{\lambda c}\gamma_{\lambda c'}}{E_{\lambda} - E - i\gamma_{\lambda\gamma}^2}, \tag{4}$$

where, the subscripts c and c' represent only particle channels. The sum over λ includes an infinite number of levels (i.e.,

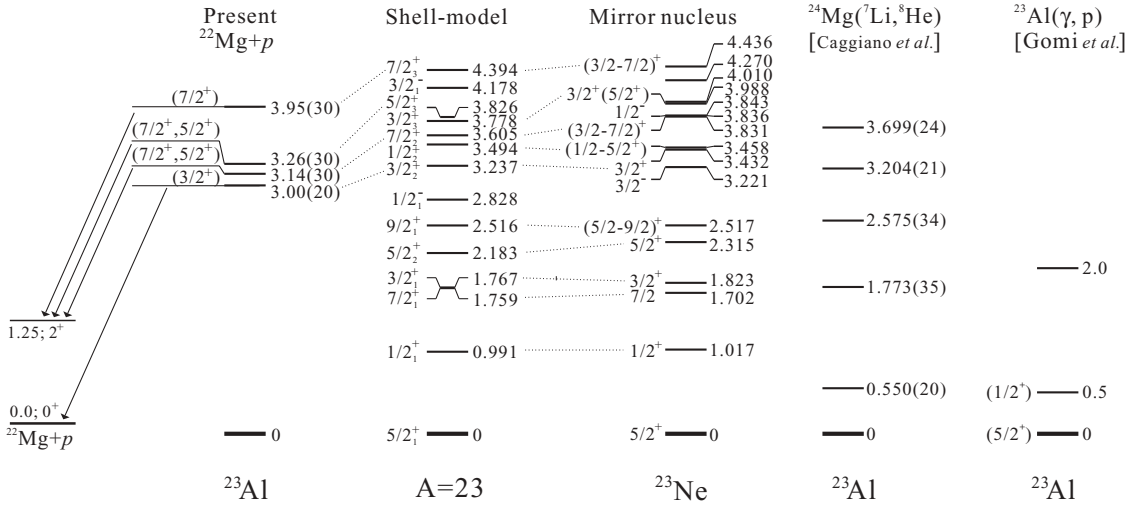

FIG. 4. New level scheme in ^{23}Al proposed in this work. The calculated levels together with the previously observed levels [1,5,6] and the mirror levels [11] are shown for comparison. (Energy in MeV).

resonances); for practical purposes, this number is of course truncated to a finite value, and the effect of the omitted levels is approximated either by large distant levels or by a parametrized R^{ext} as give in the SAMMY manual. We have neglected the effect of the omitted levels in the analysis, since it is very difficult, as we tried, to observe such a small effect in the present statistics and energy-resolution level. E_λ is the resonance energy, and the quantity $\gamma^2_{\lambda\gamma}$ is called the reduced capture width. The γ width Γ^γ_λ is given in terms of the reduced capture width amplitude (or γ width amplitude) $\gamma_{\lambda\gamma}$ as $\Gamma^\gamma_\lambda = 2\gamma^2_{\lambda\gamma}$. The particle width is defined as $\Gamma_{\lambda c} = 2\gamma^2_{\lambda c} P_\ell$, and $\gamma^2_{\lambda c}$ is referred to as the reduced particle width. Here, we assume that the γ widths Γ^γ_λ are negligible compared to the particle widths $\Gamma_{\lambda c}$. The Coulomb penetrability is given by

$$P_\ell = \frac{kR}{\left(F^2_\ell + G^2_\ell\right)_{|R}}, \tag{5}$$

where k is the wave number, $k = \sqrt{2\mu E_{\text{c.m.}}}/\hbar$ (μ is the reduced mass). F_ℓ and G_ℓ are the regular and irregular Coulomb functions, respectively. The channel (or interaction) radius is given by $R = 1.4(A_t^{1/3} + A_p^{1/3})$ fm [27]; and A_t, A_p are the mass numbers of the target and projectile, respectively. Actually, the R-matrix fitting result is not very sensitive to the choice of radius, e.g., the resultant χ^2/N value is changed by less than 2% in the 1.2∼1.6 fm range. The choice of radius has minor effect on the rather large uncertainties in both the excitation energy and the width.

Because the present version of SAMMY can only treat the differential elastic and inelastic scattering types separately rather than simultaneously, the interference between elastic and inelastic resonances is not included in the present work.

1. Elastic scattering

Since spin-parity of the proton is $J^\pi = 1/2^+$ and that of the ground state in ^{22}Mg is 0^+, the channel spin is determined uniquely to be $s = 1/2$. For the state at $E_x = 3.00$ MeV, only d-wave fits can reproduce the experimental data well, as shown in Fig. 5. Therefore, a spin-parity of $(5/2^+, 3/2^+)$ is assigned to this state. An s-wave fit is also shown for comparison. But a p-wave assignment is unlikely because of its negative-peak (dip) shape. The proton partial width is determined to be $\Gamma_p = 32 \pm 5$ keV for $J^\pi = 3/2^+$, and $\Gamma_p = 17 \pm 3$ keV for $J^\pi = 5/2^+$. The excitation energy is determined to be $E_x = 3.00 \pm 0.02$ MeV, whose uncertainty includes both systematic and fitted uncertainties. In addition, it seems that there is a "resonant shape" at E_x around 3.1 MeV, but it cannot be fitted reasonably by any ℓ values. This might be due to the poor statistics. The resonant properties have been listed in Table I.

2. Inelastic scattering

The inelastic scattering data were reanalyzed applying the kinematics appropriate to the inelastic scattering that was observed. The first excited state in ^{22}Mg has $J^\pi = 2^+$, and the channel spin has two values now: $s = 5/2$ and 3/2. Therefore, the situation is getting complicated. R-matrix fits have been attempted with all possible allowed spin-parity combinations for the states at 3.14 and 3.26 MeV. Here, only those probable

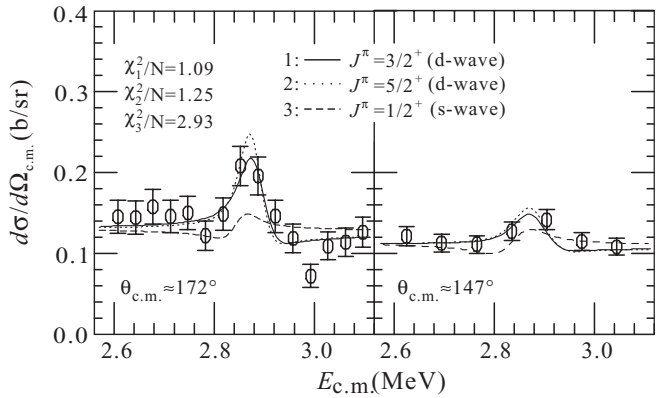

FIG. 5. R-matrix analyses for ^{22}Mg+p elastic scattering at $E_x = 3.00$ MeV.

TABLE I. Resonant properties determined in this work, together with spectroscopic factors and the proton partial widths calculated by the shell model. See text for details.

E_x(MeV)	J^π(expt)	J^π_n(calc)	$\Gamma^{\rm expt}_{p,(p')}$(keV)	$\Gamma^{\rm calc}_{p,(p')}$(keV)	ℓ	C^2S to g.s.		C^2S to 1st excited state		
						$1d_{5/2}$	$1d_{3/2}$	$1d_{5/2}$	$d_{3/2}$	$2s_{1/2}$
3.00	$(3/2^+)$	$3/2^+_2$	p: 32(5)	44	2		0.28			
			p':	5	0			0.005	0.059	0.018
3.14	$(7/2^+, 5/2^+)$	$7/2^+_2$	p: 2–5		4					
			p': 30(20)[a]	6	2			0.024	0.324	
3.26	$(7/2^+, 5/2^+)$	$5/2^+_3$	p: 2–5	3	2	0.01				
			p': 30(20)[a]	10	0			0.010	0.033	0.023
3.95	$(7/2^+)$	$7/2^+_3$	p: 20(10)		4					
			p': 30(20)	18	2			0.002	0.180	

[a]Assuming 5-keV elastic proton width.

results are shown in Fig. 6. The ℓ, s values for different J^π values are listed in Table II. In the present work, the ℓ, s combination for a given J^π value is identical. It can be seen that several combinations of spin-parity assignment can explain these two structures reasonably because of the poor counting statistics. Thus, a spin-parity of (7/2, 5/2) is tentatively assigned to the states at 3.14 and 3.26 MeV. The excitation energies are determined to be 3.14 ± 0.03 and 3.26 ± 0.03 MeV, respectively.

As for elastic scattering, the amplitude of cross section is proportional to Γ_p, while for inelastic scattering, the amplitude of cross section is proportional to $\Gamma_p\Gamma_{p'}/\Gamma_{\rm tot}$ [suffixes p and p' imply the ^{22}Mg(g.s.)+p (elastic) and ^{22}Mg(2^+_1)+p (inelastic) channels, respectively]. In turn, $\Gamma_{\rm tot} \simeq \Gamma_p + \Gamma_{p'}$ (because $\Gamma_\gamma \ll \Gamma_p$ and $\Gamma_{p'}$). Thus one can determine, to a reasonable accuracy, the elastic and inelastic widths separately. The decay branches from these two states to the ground state in ^{22}Mg, which would appear at $E_{\rm c.m.} = 3.00$–3.16 MeV, were not observed in Fig. 2, and thus their elastic proton widths may be estimated to be $\Gamma_p \leqslant 5$ keV (the estimated limit of the experiment). If Γ_p is fixed at this value, the proton inelastic partial widths are fitted to be $\Gamma_{p'} = 30 \pm 20$ keV. The resulting χ^2/N values are not very sensitive to $\Gamma_{p'}$ within the estimated uncertainties. On the other hand, if Γ_p is less than 2 keV, R-matrix fits cannot explain the inelastic cross section. Therefore, these two states are concluded to have elastic scattering widths of $2 \leqslant \Gamma_p \leqslant 5$ keV. As seen in Fig. 6(b), the fits having $\Gamma_p = 5$ keV, $\Gamma_{p'} = 30$ keV, with $J^\pi = 7/2^+$ assignments for both states, are indicated by the solid line (labeled as No. 9); although not the best fit, it is a reasonable candidate because of the low statistics.

As for the 3.95 MeV state, the R-matrix fits with $J^\pi = (7/2, 5/2^-)$ reproduce the experimental data most reasonably as shown in Fig. 7. An excitation energy of 3.95 ± 0.03 MeV is determined for this state. The proton partial widths are determined to be $\Gamma_p = 20 \pm 10$ keV and $\Gamma_{p'} = 30 \pm 20$ keV, respectively. The experimental data in the region of 3.9 MeV were affected by contaminants, and thus the above-discussed restriction on Γ_p cannot be made for this state. All the resonant properties for these inelastic scattering states are summarized in Table I.

TABLE II. Combinations of spin-parity assignments for the 3.14- and 3.26-MeV states and the corresponding χ^2/N values derived from the R-matrix analysis. (The ℓ, s values listed in parentheses are for the exit channels, and the ℓ, s combinations for one given J^π value are the same.)

Group	3.14-MeV (ℓ; s)	3.26-MeV (ℓ; s)	χ^2/N[a]
1	$7/2^+$ (2; 3/2)	$7/2^+$ (2; 3/2)	0.94, 0.48
2	$5/2^+$ (0; 5/2)	$5/2^+$ (0; 5/2)	1.04, 0.52
3	$3/2^+$ (0; 3/2)	$3/2^+$ (0; 3/2)	1.26, 0.69
4	$1/2^+$ (2; 3/2)	$1/2^+$ (2; 3/2)	1.55, 0.99
5	$1/2^-$ (1; 3/2)	$1/2^-$ (1; 3/2)	1.55, 0.99
6	$7/2^-$ (1; 5/2)	$7/2^-$ (1; 5/2)	0.86, 0.44
7	$5/2^-$ (1; 3/2)	$5/2^-$ (1; 3/2)	0.86, 0.44
8	$3/2^-$ (1; 3/2)	$3/2^-$ (1; 3/2)	1.73, 0.96
9[b]	$7/2^+$ (2; 3/2)	$7/2^+$ (2; 3/2)	0.96, 0.56
10	$7/2^+$ (2; 3/2)	$5/2^+$ (0; 5/2)	0.96, 0.48
11	$5/2^+$ (0; 5/2)	$7/2^+$ (2; 3/2)	1.06, 0.49

[a]For SET1($\theta_{\rm c.m.} \approx 172^\circ$) and SET2($\theta_{\rm c.m.} \approx 147^\circ$), respectively.
[b]The elastic and inelastic proton widths are fixed at $\Gamma_p = 5$ keV and $\Gamma_{p'} = 30$ keV, respectively.

IV. MODEL CALCULATIONS

A shell-model calculation for the $A = 23$ nucleus has been performed with the shell-model code OXBASH [29]. The calculation was carried out in a large model space (*spsdpf*) using an isospin-conserving WBT interaction of Warburton and Brown [30]. This procedure allows a consistent calculation for both positive ($0\hbar\omega$) and negative ($1\hbar\omega$) parity states with the same interaction within the same model space. All states below 7.5 MeV with $J \leqslant 9/2$ were included in the calculation. In addition, for comparison, the positive parity states were also calculated in an *sd* model space with a Wildenthal interaction [31]. The differences in the calculated excitation energies by the two procedures are less than 10 keV. Additionally, to calculate the single-particle spectroscopic factors, the states in the ^{22}Mg core were also studied within the *spsdf* model space and the WBT interaction.

The calculated levels in the $A = 23$ nucleus are listed in Table III and displayed in Fig. 4. The calculated energies of

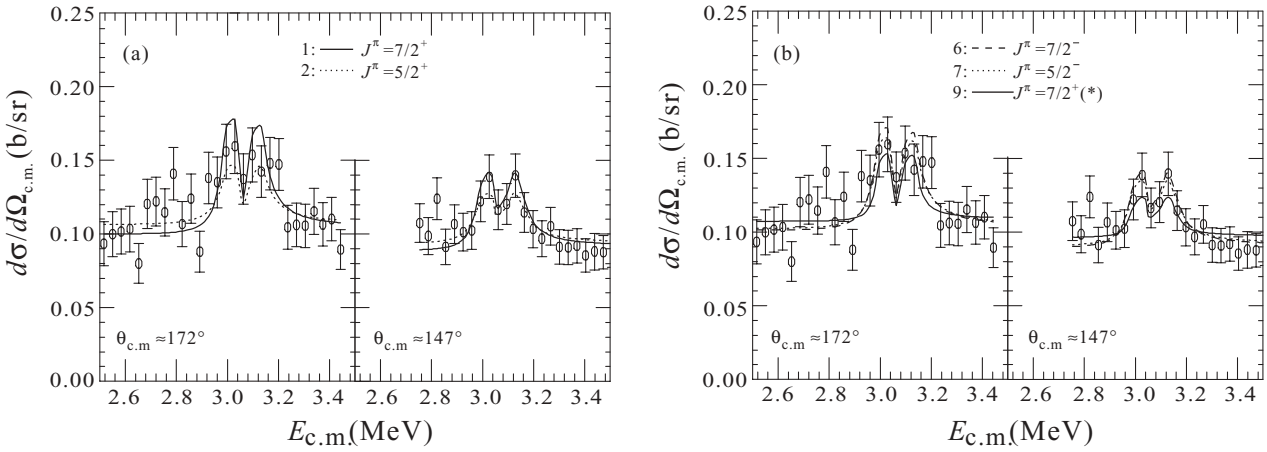

FIG. 6. *R*-matrix analyses for ^{22}Mg*$(2_1^+)+p$ inelastic scattering at $E_x = 3.14$ and 3.26 MeV.

positive states agree very well with those observed in ^{23}Ne [11]. As for the negative parity states, the discrepancies are very large. The calculated C^2S factors are also in good agreement with those determined from the (d, p) reaction [32] except for the 1.823 and 3.836 MeV states (see Table III). As for the 2.517 MeV state in ^{23}Ne, the compilations [11,33] assigned it with $J^\pi = (5/2, 7/2)^+$. This assignment was based on the assumption that the ^{23}F$(\beta^-)^{23}$Ne branches to ^{23}Ne excited states have allowed character ($\log ft = 5.9$ [33]). However, this assignment is possibly wrong as pointed out in Ref. [11]. According to calculations by the Nilsson model (with Coriolis-mixing) [34] and the OXBASH shell model, the 2.517 MeV state is tentatively assigned with $J^\pi = (5/2{-}9/2)^+$. In addition, the 3.458 MeV level might have $(1/2^+)$, from a previous work [34].

In the present work, the method for calculating proton partial width has been applied by Schiffer [28] with the result

$$\Gamma_p = C^2 S \Gamma_{\rm sp}, \tag{6}$$

where $\Gamma_{\rm sp}$ denotes the partial width of a single-particle resonance located at the same energy as the resonance of interest. This quantity can be computed numerically by solving

TABLE III. Properties of excited states in mirror ^{23}Ne [11] nucleus and those deduced from shell-model calculations.

^{23}Ne			Shell-model calculations		
E_x	J^π	C^2S[a]	E_x	J_n^π	C^2S
0	$5/2^+$	0.22 ($\ell=2$)	0	$5/2_1^+$	0.34
1.017	$1/2^+$	0.70 ($\ell=0$)	0.991	$1/2_1^+$	0.66
1.702	$7/2$[b]		1.759	$7/2_1^+$	
1.823	$3/2^+$	<0.02 ($\ell=2$)	1.767	$3/2_1^+$	0.08
2.315	$5/2^+$	0.06 ($\ell=2$)	2.183	$5/2_2^+$	0.09
2.517	$(5/2{-}9/2)^+$[,c]		2.516	$9/2_1^+$	
3.221	$3/2^-$	0.30 ($\ell=1$)	4.178	$3/2_1^-$	0.28
3.432	$3/2^+$	0.30 ($\ell=2$)	3.237	$3/2_2^+$	0.28
3.458	$(1/2, 3/2, 5/2^+)$		3.494	$1/2_2^+$	0.03
3.831	$(3/2{-}7/2)^+$		3.605	$7/2_2^+$	
3.836	$1/2^-$	0.11 ($\ell=1$)	2.828	$1/2_1^-$	0.01
3.843					
3.988	$3/2^+(5/2)^+$	0.28 ($\ell=2$)	3.778	$3/2_3^+$	0.22
4.010					
4.270					
4.436	$(3/2{-}7/2)^+$		4.394	$7/2_3^+$	

[a] S factors are from Ref. [32], transferred ℓ indicated in brackets. A 25% intrinsic uncertainty was ascribed to their DWBA analysis.
[b] $(5/2, 7/2^+)$ is adopted in Ref. [12].
[c] See text for details.

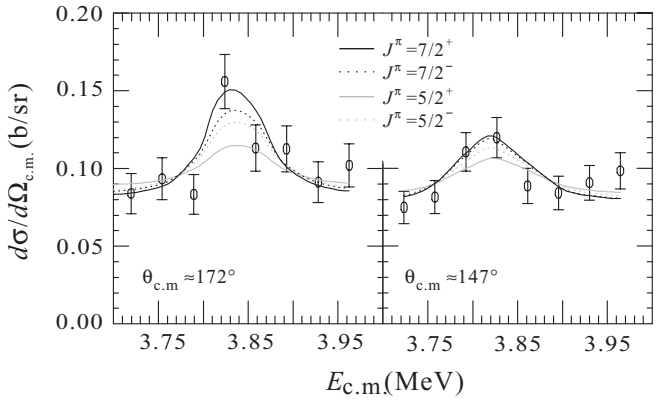

FIG. 7. Same as Fig. 6, but for $E_x = 3.95$ MeV.

the Schrödinger equation for the elastic scattering of protons by an appropriate diffuse-edge optical-model potential. The parameters have been adopted from Iliadis's work [36], i.e., values of $r_0 = 1.17$ fm, $a = 0.69$ fm, and $r_c = 1.28$ fm have been used for the Woods-Saxon optical-model potential radius and diffuseness, and the Coulomb potential radius, respectively. C^2S is the single-nucleon spectroscopic factor, which has been calculated and listed in Tables I and III. The calculated proton partial widths Γ_p are listed in Table I.

V. DISCUSSIONS

The correspondence assignments made between the experimental levels and the shell-model calculated ones are shown in Fig. 4, and the structure of the excited states in ^{23}Al is discussed in the following section.

A. 3.00 MeV state

We suggest that the 3.00 MeV state corresponds to the calculated 3.237 MeV state ($J^\pi_n = 3/2^+_2$). The predicted Γ_p value is 44 keV (see Table I), which agrees well with the experimental value of $\Gamma_p = 32 \pm 5$ keV (with $J^\pi = 3/2^+$). Therefore, a spin-parity of $J^\pi = (3/2^+)$ is most favorable to this state. The main configuration of this state may be written as $0^+ \otimes 1d_{3/2}$, where 0^+ indicates the ^{22}Mg core ground state, and the proton occupies the $1d_{3/2}$ orbit in the ^{23}Al nucleus. In comparison, the excitation energy of the $1d_{3/2}$ single-particle state is 3.43 MeV in ^{23}Ne. In ^{23}Na, the 7.890 MeV state (with $5/2^+$) may be considered as the ground state with respect to the isospin quartet states of $T = 3/2$ [33], and the 11.247 MeV state ($J^\pi = 3/2^+$, $T = 3/2$) [35] might correspond to the presently observed state. It gives an energy of 3.36 MeV ($= 11.247 - 7.890$) for the $1d_{3/2}$ single particle in ^{23}Na ($T = 3/2$).

B. 3.14, 3.26 MeV states

According to the R-matrix analysis, the most possible assignment for the 3.14 MeV state is $J^\pi = (7/2, 5/2)$, with $\pi = +$ or $-$. It can be seen that no negative parity states with $5/2^-$ and $7/2^-$ assignments are observed in the mirror nucleus (^{23}Ne) or predicted by the shell model in the present energy region (see Fig. 4). Therefore, it most likely has an assignment of $J^\pi = (7/2^+, 5/2^+)$. It possibly corresponds to the calculated 3.605 $(7/2^+_2)$ state. According to the shell-model calculations, it mainly decays to the first excited state in ^{22}Mg by a $1d_{3/2}$ proton emission rather than to the ground state, and this result is consistent with the experimental observations. The predicted proton width value is $\Gamma_{p'} = 6$ keV, which is not very far from the experimental value $\Gamma_{p'} = 30 \pm 20$ keV (within 2σ error of predicted value). Its main configuration can be written as $2^+ \otimes 1d_{3/2}$, where 2^+ implies the first excited state in the ^{22}Mg core, and the proton occupies the $1d_{3/2}$ orbit in the ^{23}Al nucleus. Likewise, the 3.26 MeV state is tentatively assigned $J^\pi = (7/2^+, 5/2^+)$, and it decays mainly to the first excited state in ^{22}Mg as well. The predicted $\Gamma_{p'}$ values are 10 and 1 keV for the $2s_{1/2}$ and $1d_{3/2}$ proton emissions, respectively. Therefore, the former is dominant in the proton emission, and the width is also close to the experimental value $\Gamma_{p'} = 30 \pm 20$ keV. Its main configuration is possibly a mixing of $2^+ \otimes 2s_{1/2}$ and $2^+ \otimes 1d_{3/2}$. Furthermore, the calculated proton width to the ground state in ^{22}Mg via a $1d_{5/2}$ decay is only about $\Gamma_p = 3$ eV, in agreement with the above restriction of $2 \leqslant \Gamma_p \leqslant 5$ keV (see Sec. III B 2).

C. 3.95 MeV state

By the R-matrix analysis, most probably the 3.95-MeV state has an assignment of $J^\pi = (7/2, 5/2^-)$. The $5/2^-$ assignment is unlikely by comparing the structures observed in the mirror nucleus and those calculated by the shell model. It has most probably an assignment of $J^\pi = (7/2^+)$. It mainly decays to the first excited state in ^{22}Mg by $1d_{3/2}$ proton emission. The predicted $\Gamma_{p'}$ value is 18 keV, which agrees well with that deduced from the R-matrix analysis of $\Gamma_{p'} = 30 \pm 20$ keV. The main configuration can be written as $2^+ \otimes 1d_{3/2}$ in the same way.

D. Other unobserved states

The previously observed 1.773 MeV state [1] is not identified in the present experiment possibly because of either the poor counting statistics or its narrow width ($\Gamma_p \sim 1$ keV). In addition, the previously observed 3.699 MeV state is also not identified because of the unresolved background contamination specifically in the present study. Here we would like to mention the previously observed 2.575 MeV state which most probably corresponds to the predicted $J^\pi = 5/2^+_2$ state (see Fig. 4). The calculated proton width to the ground state in ^{22}Mg is only about 3 keV, while that to the first excited state via a $2s_{1/2}$ proton emission may be as large as 20 keV. This "inelastic" proton-decay branch should appear around $E_{c.m.} = 1.76$ MeV with SET1 (see Fig. 2). Unfortunately, the low counting statistics prohibited our drawing a conclusion, although some small structures were observed. Additionally, in the Coulomb-dissociation study [5], a state at $E_x \sim 2$ MeV decaying to the first excited state in ^{22}Mg was observed, and it probably corresponds to this state.

E. Halo structure

It has been suggested that a proton halo structure, with $J^\pi = 1/2^+$ assignment, should exist in the ground state of ^{23}Al [7,8]. However, a recent measurement of the magnetic moment by the β-NMR method [9] has clearly shown that the ^{23}Al ground state has a normal spin-parity of $5/2^+$, and a β-decay study of ^{23}Al with β-γ coincidence measurements [10] has confirmed this normal assignment as well. The present shell-model calculation, which describes the present data well, also predicts spin-parities of $5/2^+$ and $1/2^+$ for the ground and first excited states in ^{23}Al (see Fig. 4), respectively. Therefore the present result supports this normal spin-parity assignment as well. According to the shell-model calculation, the first excited state in $A = 23$ nuclei has a very good single-particle character of $s_{1/2}$ with $C^2S = 0.70$; therefore, the proton halo structure may appear in the first excited state instead of the ground state.

VI. ASTROPHYSICAL REACTION RATE

The stellar reaction rate of ^{22}Mg$(p,\gamma)^{23}$Al had been calculated in the previous work [1,2]. However, it should be noted that there are some typographical errors in Eqs. (2) and (3) of Ref. [1]. Furthermore, we could not reproduce the previous resonant reaction rates as listed in their Table V and Fig. 5 [1]. It is likely that the proton energy $E_p(=\frac{23}{22}E_r$, i.e., 0.423 MeV) was used in their calculation instead of the resonant one E_r (i.e., 0.405 MeV). In addition, the experimental value of Γ_γ [6] is available now. Therefore we would like to reevaluate this reaction rate here.

The nonresonant (i.e., direct capture) reaction rate can be calculated by [37]

$$\langle \sigma v\rangle = \left(\frac{8}{\pi\mu}\right)^{1/2}\frac{1}{(kT)^{3/2}} \times \int_0^\infty S(E)\exp\left[-\frac{E}{kT}-\frac{b}{E^{1/2}}\right]dE. \quad (7)$$

If the $S(E)$ factor is nearly a constant over the Gamow window, the nonresonant reaction rate can be approximated in a form [37]

$$\langle \sigma v\rangle_{\rm dc} = 1.30\times10^{-14}\left(\frac{Z_1Z_2}{A_r}\right)^{1/3} T_9^{-2/3} S_{\rm eff} \times \exp\left[-4.2487\left(\frac{Z_1^2Z_2^2A_r}{T_9}\right)^{1/3}\right] [\mathrm{cm^3\ s^{-1}}], \quad (8)$$

and the effective S factor is given, in units of MeV b, as

$$S_{\rm eff} = S_0\left(1+\frac{5}{12\tau}\right) = S_0\left(1+\frac{5T_9^{1/3}}{50.984\left(Z_1^2Z_2^2A_r\right)^{1/3}}\right), \quad (9)$$

where the factor $(1 + 5/12\tau)$ reflects the correction factor $F(\tau)$ for the asymmetry of the Gamow peak [37]. The assumed constant S factor (S_0) has been calculated in the work of Caggiano *et al.* in which S_0 represented an averaged value of the calculated $S(E)$ over the characteristic energy range of novae burning, i.e., 0.1–0.3 MeV. Additionally, if the $S(E)$ factor is described by a slowly varying function of energy E rather than by a constant, it can be expanded in a Taylor series,

$$S(E) = S(0) + \dot{S}(0)E + \tfrac{1}{2}\ddot{S}(0)E^2 + \cdots. \quad (10)$$

As a result, the effective S factor can be expressed as

$$S_{\rm eff}(E_0) = S(0)\left[1+\frac{5}{12\tau}+\frac{\dot{S}(0)}{S(0)}\left(E_0+\frac{35}{36}kT\right) + \frac{1}{2}\frac{\ddot{S}(0)}{S(0)}\left(E_0^2+\frac{89}{36}E_0kT\right)\right] \quad (11)$$

in a Gaussian function approximation [37,38], and can either be expressed as

$$S_{\rm eff}^{\rm LFA}(E_0) = S(0)\left[1+\frac{5}{12\tau}+\frac{\dot{S}(0)}{S(0)}\left(E_0+\frac{5}{36}kT\right) + \frac{1}{2}\frac{\ddot{S}(0)}{S(0)}\left(E_0^2+\frac{53}{36}E_0kT\right)\right] \quad (12)$$

in a Lorentzian function approximation [39]. Again, the first two terms inside the brackets reflect the correction factor for the asymmetry of the Gamow peak. The remaining terms result from the assumption that $S(E)$ is a slowly varying function of energy, and they are generally much more important than the second term [37]. Therefore, Eqs. (11) and (12) cannot be simply written in the form of Eq. (9) in this case.

In the present work, the contribution to the ^{22}Mg$(p,\gamma)^{23}$Al rate from direct capture into ground state in ^{23}Al has been calculated with a potential model [40] using a Woods-Saxon nuclear potential (central plus spin orbit) and a Coulomb potential of a uniform charge distribution. For consistency, the parameters are again taken from Ref. [36], i.e., $r_0 = 1.17$ fm, $a = 0.69$ fm, and $r_c = 1.28$ fm for the Woods-Saxon optical-model potential radius and diffuseness, and the Coulomb potential radius, respectively. The Woods-Saxon potential V_0 is varied to reproduce the bound energy of the ground state in ^{23}Al. As for the spin-orbit potential, the parameters are $V_{\rm so} = -6.41$ MeV, $r_{\rm so} = 1.06$ fm, and $a_{\rm so} = 0.66$ fm, respectively, which are the averaged values from the literature [41–44]. The calculated averaged values of $S(E)$ over the energy range of 0.1–0.3 MeV are 6.12×10^{-4} MeV b for the $p\to d$ transition and 6.04×10^{-5} MeV b for the $f\to d$ transition, respectively. The differences are very small, about 8.4% and 14.2% compared to the previous ones [1], and the $S(E)$ values are changed by about 9% and 14% within this energy range for these two cases. However, the $S(E)$ values are changed by about 50% and 107% over the energy range of 0.1–1.0 MeV for these two cases. Therefore, the approximation made in Eq. (9) is not very appropriate beyond the novae temperature. In the present calculation, the direct capture (DC) rate has been calculated directly from Eq. (7) by using the calculated $S(E)$ factors. The spectroscopic factor (i.e., $C^2S = 0.34$) is taken from the previous work [1,2] and is also reproduced in our shell-model calculation. The present DC rates are listed in Table IV and are compared to the previous ones.

TABLE IV. Reaction rates of ^{22}Mg$(p,\gamma)^{23}$Al reaction in units of cm^3/mole s as a function of temperature. Listed are the revised and the previous [1] resonant (only due to $E_r = 0.405$ MeV resonance) and DC rates together their corresponding ratios. Ratio$^{\text{Total}}$ represents the ratio between the revised total rate and the previous one.

T(GK)	Resonant rate			DC rate			Ratio$^{\text{Total}}$
	$N_A\langle\sigma v\rangle^{\text{res}}_{\text{revised}}$	$N_A\langle\sigma v\rangle^{\text{res}}_{\text{previous}}$	Ratio$^{\text{res}}$	$N_A\langle\sigma v\rangle^{\text{DC}}_{\text{revised}}$	$N_A\langle\sigma v\rangle^{\text{DC}}_{\text{previous}}$	Ratio$^{\text{DC}}$	
0.10	1.44×10^{-20}	1.32×10^{-21}	10.9	1.67×10^{-13}	1.70×10^{-13}	1.0	1.0
0.15	4.98×10^{-14}	9.20×10^{-15}	5.4	5.11×10^{-11}	5.13×10^{-11}	1.0	1.0
0.20	8.16×10^{-11}	2.14×10^{-11}	3.8	1.88×10^{-9}	1.87×10^{-9}	1.0	1.0
0.30	1.12×10^{-7}	4.16×10^{-8}	2.7	1.71×10^{-7}	1.66×10^{-7}	1.0	1.4
0.40	3.66×10^{-6}	1.61×10^{-6}	2.3	2.92×10^{-6}	2.81×10^{-6}	1.0	1.5
0.50	2.74×10^{-5}	1.34×10^{-5}	2.1	2.20×10^{-5}	2.09×10^{-5}	1.1	1.4
0.60	1.00×10^{-4}	5.25×10^{-5}	1.9	1.03×10^{-4}	9.62×10^{-5}	1.1	1.4
0.70	2.43×10^{-4}	1.34×10^{-4}	1.8	3.51×10^{-4}	3.24×10^{-4}	1.1	1.3
0.80	4.60×10^{-4}	2.64×10^{-4}	1.7	9.69×10^{-4}	8.77×10^{-4}	1.1	1.3
0.90	7.41×10^{-4}	4.37×10^{-4}	1.7	2.29×10^{-3}	2.04×10^{-3}	1.1	1.2
1.00	1.07×10^{-3}	6.44×10^{-4}	1.7	4.79×10^{-3}	4.21×10^{-3}	1.1	1.2
1.50	2.78×10^{-3}	1.80×10^{-3}	1.6	6.57×10^{-2}	5.23×10^{-2}	1.3	1.3
2.00	3.95×10^{-3}	2.65×10^{-3}	1.5	3.46×10^{-1}	2.52×10^{-1}	1.4	1.4

The resonant capture rate for isolated, narrow resonance is given by

$$\langle\sigma v\rangle_{\text{res}} = 2.557 \times 10^{-19}(A_r T_9)^{-3/2}\omega\gamma \times \exp\left(-\frac{11.605E_r}{T_9}\right)[\text{cm}^3 s^{-1}], \quad (13)$$

where the reduced mass A_r (in amu) is given by $A_b A_t/(A_b + A_t)$, and A_b and A_t are defined in Eq. (1). The resonance strength $\omega\gamma$ is in eV, and E_r in MeV. Wiescher *et al.* [2] computed the γ width from the reduced $E2$ transition probability $B(E2)$ for the γ decay of the first excited state ($\frac{1}{2}^+$, $E_x = 0.47 \pm 0.04$ MeV) to the ground state ($\frac{5}{2}^+$) with a shell model, and it yielded $\Gamma_\gamma = 2.5^{+1.2}_{-0.9} \times 10^{-7}$ eV. The Weisskopf-unit γ width (in eV) is known as $\Gamma^W_\gamma(E2) = 4.9 \times 10^{-8} A^{4/3} E^5_\gamma$ [45]. Therefore, the γ width is calculated to be $\Gamma_\gamma = 5.49 \times 10^{-7}$ eV for the new excitation energy (i.e., 0.550 MeV) in ^{23}Al as measured by Caggiano *et al.* If we take the averaged excitation energy (i.e., 0.528 MeV [1]), the γ width is calculated to be $\Gamma_\gamma = 4.5 \times 10^{-7}$ eV. However, for a reliable calculation, an experimental value of $\Gamma_\gamma = 7.2 \times 10^{-7}$ eV (with 20% uncertainty) [6], which is about a factor of 1.6 larger than the calculated one, has been used in the present work. The revised resonant reaction rates (only due to $E_r = 0.405$ MeV resonance) have been listed in Table IV together with those calculated in the previous work for comparison.

According to the present reevaluation, the revised resonant rate is much higher than previously expected at lower temperature, by about one order of magnitude at $T_9 = 0.1$. The DC rate is increased up to 40% at $T_9 = 2$, although it does not change at the novae temperature. As a result, the total reaction rate is increased by about 40% beyond $T_9 = 0.3$.

The calculated rates are shown in Fig. 8, where the black solid lines show the upper and lower limits for resonant contribution from $E_r = 0.405 \pm 0.027$ MeV resonance due to the uncertainties in the resonance locations as well as in the resonant strength. The presently calculated direct capture rate and the previous results obtained with the NON-SMOKER code, are also shown for comparison. The DC contribution dominates in the rate below temperature $T_9 = 0.2$, and both direct and resonant captures contribute significantly to the rate beyond this temperature up to $T_9 = 1.0$.

In addition, for completeness, the resonant reaction rates for states at 1.773, 2.575, and 3.00 MeV have been calculated, although they are too high in novae temperature. The relevant parameters were calculated and are listed in Table V. The $B(E2)$ and $B(M1)$ values for the γ transition to the ground state in ^{23}Al were calculated by the OXBASH code with the SD model space and the Wildenthal interaction. Here, we assume the mixing ratio of $E2$ and $M1$ transitions is unity. The γ widths have been calculated, i.e., $\Gamma_\gamma(E2) = \frac{B(E2)}{B^W(E2)}\Gamma^W_\gamma(E2)$ for the $E2$ transition,

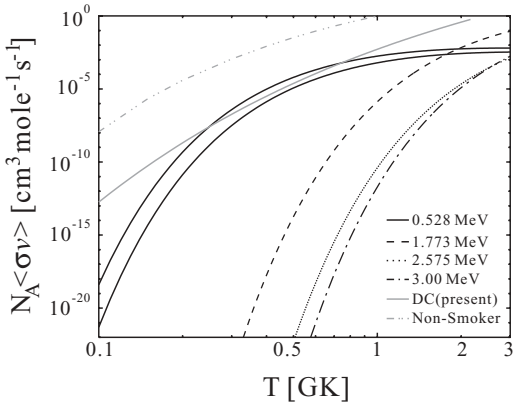

FIG. 8. Revised reaction rates for ^{22}Mg$(p,\gamma)^{23}$Al reaction. Two black solid lines show the upper and lower limits for resonant contribution from the first excited state at 0.528 MeV. The presently calculated DC rate and the rate [1] obtained with the NON-SMOKER code are shown for comparison. Additionally, three other resonant contributions are indicated as well. See text for details.

TABLE V. Relevant parameters for selected states in ^{23}Al used in calculating the reaction rates (E_x in MeV).

E_x^{expt}[a]	$B(E2)$ (e^2 fm^4)	$B(M1)$ (μ_N^2)	Γ_γ (eV)[b]	$\omega\gamma$ (eV)
0.528 [1]	20.4		$(7.2 \pm 1.5) \times 10^{-7}$	$(7.2 \pm 1.5) \times 10^{-7}$
1.773 [1]	10.3	2.4×10^{-2}	8.3×10^{-4}	1.7×10^{-3}
2.575 [1]	5.1	1.3×10^{-5}	1.9×10^{-4}	5.7×10^{-4}
3.00[c]	2.4	1.1×10^{-2}	1.9×10^{-3}	3.8×10^{-3}

[a]Used in calculating the γ-transition width.
[b]Data from Ref. [6] for the first excited state, $\Gamma_\gamma = [\Gamma_\gamma(E2) + \Gamma_\gamma(M1)]/2$ for the latter three states.
[c]From present work.

and $\Gamma_\gamma(M1) = \frac{B(M1)}{B^W(M1)}\Gamma_\gamma^W(M1)$ for the $M1$ transition, where the Weisskopf units are $B^W(E2) = \frac{1}{4\pi}(\frac{3}{2+3})^2 R^4 \simeq 6.04e^2$ fm^4 ($R = 1.34A^{1/3}$ fm) and $B^W(M1) = \frac{10}{\pi}(\frac{3}{1+3})^2 \simeq 1.79\mu_N^2$, and the Weisskopf-unit γ width (in eV) for the $M1$ transition is $\Gamma_\gamma^W(M1) = 2.1 \times 10^{-2} E_\gamma^3$ [45]. Since $\Gamma_p \gg \Gamma_\gamma$ in the present case, the resonance strength simply becomes $\omega\gamma = \omega\Gamma_\gamma$. The corresponding curves are shown in Fig. 8. It is very clear that these high-lying resonances do not affect the total reaction rate at any temperature of interest.

VII. CONCLUSIONS

We have studied for the first time the resonant elastic and inelastic scattering of ^{22}Mg+p using a radioactive ion beam of ^{22}Mg with a thick hydrogen target. By analyzing the scattering data at different angles, a new resonant state in ^{23}Al due to elastic scattering has been identified at $E_x = 3.00 \pm 0.02$ MeV; and three other states at 3.14, 3.26, and 3.95 MeV have also been established, which mainly decay to the first excited state of ^{22}Mg by the proton emissions. There, the state at 3.95 MeV is also newly observed. Their resonance parameters have been determined by the R-matrix analysis as well as shell-model calculations. Qualitatively, the presently observed states can be explained in a valence particle coupled with a core (in ground or excited state) picture. The rate of the ^{22}Mg$(p,\gamma)^{23}$Al reaction has been reevaluated in the present work. The revised total reaction rate is about 40% greater than the previous result for temperatures beyond $T_9 = 0.3$. In addition, the NON-SMOKER model, whose results are largely overestimated, is not applicable in this case because of the low level density in ^{23}Al.

The present spectroscopy of single-particle states built on an excited core made via thick target method resonant (elastic and inelastic) scattering has proven to be a very simple technique for deducing excited-core coupled single-particle components. The resonant inelastic scattering events have been identified by determining the kinematics energy shifts at different scattering angles. This kinematics analysis approach in combination with a γ-ray coincidence measurement [46] can provide abundant spectroscopic information for nuclear physics as well as for nuclear astrophysics.

ACKNOWLEDGMENTS

We thank Y. Ohshiro for the ion source development and N. Yamazaki for the CRIB development. We also thank the RIKEN staff for their operation of the AVF cyclotron. This work is supported by Grant-in-Aid for Science Research from the Japanese Ministry of Education, Culture, Sports, and Technology under Contract Nos. 13440071 and 14740156, and by the Grants-in-Aids for the JSPS (1604055).

[1] J. A. Caggiano *et al.*, Phys. Rev. C **64**, 025802 (2001).
[2] M. Wiescher *et al.*, Nucl. Phys. **A484**, 90 (1988).
[3] B. Blank *et al.*, Z. Phys. A **357**, 247 (1997).
[4] S. Czajkowski *et al.*, Nucl. Phys. **A616**, 278c (1997).
[5] T. Gomi *et al.*, Nucl. Phys. **A718**, 508c (2003).
[6] T. Gomi *et al.*, Nucl. Phys. **A758**, 761c (2005).
[7] X. Z. Cai *et al.*, Phys. Rev. C **65**, 024610 (2002).
[8] H. Y. Zhang *et al.*, Nucl. Phys. **A722**, 518c (2003).
[9] A. Ozawa *et al.*, Phys. Rev. C **74**, 021301(R) (2006).
[10] V. E. Iacob *et al.*, Phys. Rev. C **74**, 045810 (2006).
[11] P. M. Endt, Nucl. Phys. **A633**, 1 (1998).
[12] R. B. Firestone, Nucl. Data Sheets **108**, 1 (2007).
[13] G. Audi and A. H. Wapstra, Nucl. Phys. **A565**, 1 (1993).
[14] R. D. Gehrz *et al.*, Astrophys. J. Lett. **298**, L47 (1985).
[15] A. F. Iyudin *et al.*, Astron. Astrophys. **300**, 422 (1995).
[16] C. Iliadis *et al.*, Astrophys. J. Suppl. **142**, 105 (2002).
[17] S. Kubono *et al.*, Eur. Phys. J. A **13**, 217 (2002).
[18] Y. Yanagisawa *et al.*, Nucl. Instrum. Methods A **539**, 74 (2005).
[19] Joint Venture of CNS and RIKEN, called the AVF Upgrade Project (unpublished).
[20] J. J. He *et al.* (in preparation).
[21] H. Kumagai *et al.*, Nucl. Instrum. Methods A **470**, 562 (2001).
[22] S. Kubono, Nucl. Phys. **A693**, 221 (2001).
[23] J. F. Ziegler *et al.*, *The Stopping and Range of Ions in Solids* (Pergamon, New York, 1985).
[24] A. M. Lane and R. G. Thomas, Rev. Mod. Phys. **30**, 257 (1958).
[25] N. M. Larson, A Code System for Multilevel R-Matrix Fits to Neutron Data Using Bayes' Equations, ORNL/TM-9179/R5, 2000 (unpublished).
[26] W. C. Reich and M. S. Moore, Phys. Rev. **111**, 929 (1958).
[27] C. Ruiz, T. Davinson, F. Sarazin *et al.*, Phys. Rev. C **71**, 025802 (2005).
[28] J. P. Schiffer, Nucl. Phys. **46**, 246 (1963).
[29] B. A. Brown *et al.*, MSU-NSCL Rep. No. 1289 (unpublished).

[30] E. K. Warburton and B. A. Brown, Phys. Rev. C **46**, 923 (1992).
[31] B. H. Wildenthal, Prog. Part. Nucl. Phys. **11**, 5 (1984).
[32] A. J. Howard, J. G. Pronko, and C. A. Whitten, Nucl. Phys. **A152**, 317 (1970).
[33] P. M. Endt, Nucl. Phys. **A521**, 1 (1990).
[34] J. E. Christiansson, Phys. Scr. **10**, 65 (1974).
[35] P. M. Endt and C. Van Der Leun, Nucl. Phys. **A310**, 1 (1978).
[36] C. Iliadis, Nucl. Phys. **A618**, 166 (1997).
[37] C. E. Rolfs and W. S. Rodney, *Cauldrons in the Cosmos*, (University of Chicago Press, Chicago, 1988).
[38] W. A. Fowler, G. R. Caughlan, and B. A. Zimmerman, Annu. Rev. Astron. Astrophys. **5**, 525 (1967).
[39] J. J. He, Eur. Phys. J. A **33**, 5 (2007).
[40] C. A. Bertulani, Comput. Phys. Commun. **156**, 123 (2003).
[41] F. G. Perey, Phys. Rev. **131**, 745 (1963).
[42] F. D. Becchetti and G. W. Greenlees, Phys. Rev. **182**, 1190 (1969).
[43] J. J. H. Menet *et al*., Phys. Rev. C **4**, 1114 (1971).
[44] R. L. Varner *et al*., Phys. Rep. **201**, 57 (1991).
[45] D. H. Wilkinson, in *Nuclear Spectroscopy*, edited by F. Ajzenberg-Selove (Academic Press, New York, 1960), Vol. B.
[46] H. Yamaguchi *et al*., AIP Conf. Proc. **847**, 275 (2006).